Proceedings of the 20th International Conference on Soil Mechanics and Geotechnical Engineering– Rahman and Jaksa (Eds)

Large scale levee failures at the Rixin section during the 2016 Meinong earthquake

Ruptures de digues à grande échelle dans la section Rixin lors du tremblement de terre de Meinong 2016

Chin-Chin Tsai, Min-Hua Chung, & Zi-Xian Yang

Department of Civil Engineering, National Chung-Hsing University, 40277, Taichung, Taiwan

Jiunn-Shyang Chiou

Department of Civil Engineering, National Taiwan University, 10617, Taipei, Taiwan

Shang-Yi Hsu

National Center for Research on Earthquake Engineering, 10617, Taipei, Taiwan

ABSTRACT: The 2016 Meinong earthquake caused serious disaster in southern Taiwan, including many liquefaction-induced damages. This study investigates the "flow-like" failure of Rixin levee during the Meinong earthquake. The failure mechanism by soil liquefaction, however, fails to explain the case of Rixin levee because the embankment and foundation are primarily composed of clayey soil. Therefore, the cyclic softening of clayey soil subjected to cyclic loading is considered as a key factor to induce the damage. It is found that when the strength of Rixin levee is reduced by about 10~15% accounting for cycle softening, the estimated displacement of the embankment is in line with the observed damage of the levee.

RÉSUMÉ : Le tremblement de terre de Meinong en 2016 a provoqué une grave catastrophe dans le sud de Taiwan, y compris de nombreux dommages induits par la liquéfaction. Cette étude examine la défaillance « en forme de flux» de la digue de Rixin lors du tremblement de terre de Meinong. Le mécanisme de rupture par liquéfaction du sol n'explique cependant pas le cas de la digue de Rixin car le remblai et les fondations sont principalement composés de sols argileux. Par conséquent, le ramollissement cyclique des sols argileux soumis à une charge cyclique est considéré comme un facteur clé pour induire les dommages. On constate que lorsque la résistance de la digue de Rixin est réduite d'environ 10~15% compte tenu de l'adoucissement du cycle, le déplacement estimé de la digue est en ligne avec les dommages observés de la digue.

KEYWORDS: Levee; cyclic softening; liquefaction; displacement; earthquake.

1 INTRODUCTION.

The Meinong earthquake struck southern Taiwan at 3:57:27.2 am on February 6, 2016, local time (world time, February 5, 07:57:26.1). The earthquake registered a local magnitude (M_L) of 6.6 [moment magnitude (Mw), 6.4] with the epicenter at 22.92° north and 120.54° east and a focal depth of 14.6 km, as measured by the Taiwan Central Weather Bureau (CWB). No significant damage was reported in the epicentral region. However, serious damage was found about 30 km away from the west of the epicenter in Tainan City, where more than 20 multi-story buildings constructed under relatively modern building design code were severely damaged. The collapse of the 16-story Wen Gun complex building (30 km from the epicenter) caused the deaths of more than 100 people. The total humanitarian loss included 116 fatalities and more than 500 injuries.

The Meinong earthquake caused widespread damage associated with liquefaction (e.g., settlement and tilt of residential buildings) even though the intensity of ground shaking was moderate. Most of the liquefaction occurred in very fine sands to very silty sands, which were located at the lower bound gradation of typical liquefiable soil (Tsai et al. 2017). The two types of significant damage to the levee of the Tseng-wen River were also suspected to be induced by soil liquefaction. A flow-type of failure caused tremendous loss of levee and large amounts of debris almost blocked the flow channel of the river. In this paper, the observed levee failure of three sections at the Rixin site during reconnaissance right after earthquake is introduced. Additional field investigation and laboratory test was performed to characterize the embankment and foundation soil. Based on this information, liquefaction, seepage, slope stability analysis, and Newmark sliding block analysis were performed to gain insight of the failure mechanism. Moreover, the cyclic softening of clayey soil subjected to cyclic loading is considered in the analysis.

2 GORUND SHAKING AND LEVEE FAILURE

2.1 *Ground Shaking*

Three strong motion stations are close to the site as listed in Table 1. The closest station is CHY085 station, which is 2.78 km from the site and measured PGA is 233 gal. The other two CHY062, CHY089 (11.9 and 8.7 km away) has higher PGA because they are close to epicenter. The ground shaking is judged to be approximate 0.28g based on the interpolation of these stations.

Table 1 Strong motion station and record near the Rixin sections.

Station	Latitude	Longitude	PGA (gal)
CHY058	123.08	23.732	233
CHY062	120.327	23.171	426
CHY089	120.464	23.727	394

2.1 *Levee failure*

Three flow–type failures in the Rixin embankment were located near the intersection of High way No. 3 and the Tseng-wen River as displayed in Figure 1. The height of embankment at the Rixin Section was approximately 15 m, which was constructed by a 1:2 slope with a 2 m setback at the middle. The slope was protected by a 30-cm unreinforced concrete slab.

As reported by Tsai et al. (2017), two large scale failures, R0+850 and R1+200, occurred at the upstream of Highway No. 3, as shown in Figure 1. The dimension of R1+200 was approximately 150 m by 75 m, whereas the dimension of R0+850 was approximately 75 m by 75 m. Another failure, R1+700, was located at the downstream adjacent to the Highway No. 3 Tseng-wen River Bridge. The dimension of the R1+700 area was approximately 100 m by 125 m. As shown in Figure 2, the access road on the crest and the entire section of embankment at R1+200 and R1+700 were gone after the earthquake. However, the landside ground of the levee did not exhibit significant deformation at these two locations. By contrast, the failure occurred mostly on the floodplain and ceased at the toe of the embankment at R0+850. The debris of sliding mass almost blocked the Tseng-wen River at three failure locations.

The mode of slope failure here differed from the typical slope failure that exhibits a limited sliding distance. By contrast, the embankment slumped over a wide area because of the significant loss of strength from earthquake loading but the landside ground remained intact, indicating no liquefaction associated failures occurred there. The visible run out distances were more than twice the height of the embankment. However, whether the failure was due to liquefaction or not is not clear only with the observed feature of lateral spreading. During the reconnaissance by Tsai et al. (2017), no manifestation of liquefaction (e.g., soil boil) was observed. Nevertheless, at R1+200 and R1+700, the groundwater could be high in the embankment because of the unpaved irrigation channel and the rice farm (similar to a pond) behind the R1+200 and R1+700 sections, respectively, as shown in Figure 2. Because of the seepage, several ponds filled with mud and sand mixture were developed on the debris (Figure 2a), which supported the hypothesis of seepage problem to induce the failure.

At R0+850, the embankment could be dry because no irrigation channel or rice farm existed behind. As a result, the failure here only extended on the flood plain, which was different from the other two locations where the entire embankment failed due to the seepage problem. The flood plain at R0+850 was gentle with a slope of less than 7.5°. Therefore, sudden loss of strength was required to trigger this flow-type failure.

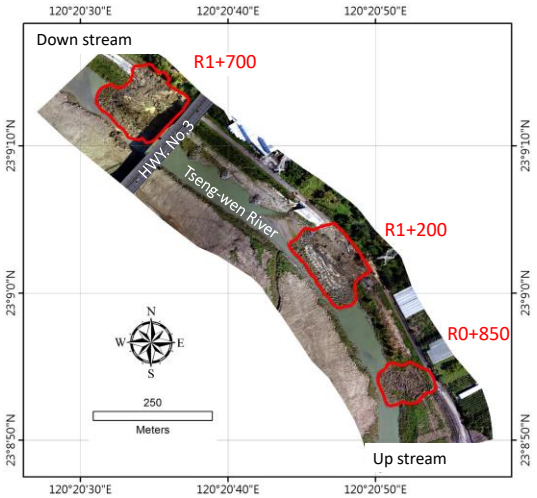

Figure 1. Orthophoto of the failure area at the Rixin section (Tsai et al. 2017).

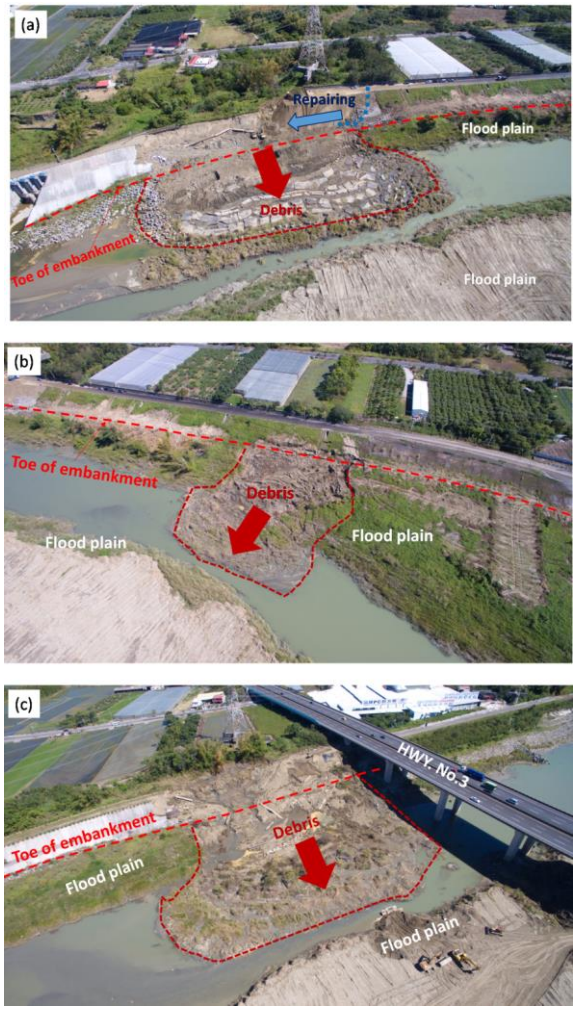

Figure 2. Arial photos of the levee failure at the Rixin sections (a) R1+200, (b) R0+850, (c) R1+700 (Tsai et al. 2017).

3 FIELD INVESTIFATION AND SUBSURFACE CHARACTERIZATION

3.1 *Field investigation*

Two types of in-situ techniques were conducted after the earthquake to characterize subsurface condition, including standard penetration tests (SPT) and cone penetration tests with pore pressure measurement and downhole seismic testing (SCPTu). SPT blowcount (SPT-N) was measured by an automatic hammer falling system every 1.5 m or at the depth of notable discontinuity during drilling. However, energy ratio was not measured during the test. Undisturbed soil samples were also retrieved with modified hydraulic piston samplers for static and dynamic laboratory tests. On the other hand, the CPT sounding was performed with a standard penetration rate of 20 mm per second (PR=20 mm/s). The downhole shear wave velocity (Vs) tests were measured by SCPT every meter. Total 3 borings and 2 CPTs were drilled at the vicinity of three failure locations as shown in Figure 3. Based on these information and the boring drilled before the earthquake in 2012 (denoted as A). The cross sections of R1+200, R1+700m, and R0+850 were characterized and shown in Figure 3.

3.2 *Subsurface characterization*

At R1+200, additional sand fill was placed on the original ground to form the current embankment mainly composed of loose sand.

The foundation soil is thick low to medium plastic clay with PI ranging from 16~27 and extends to the floodplain. The measured groundwater table was high at this section due to an unpaved irrigation channel behind the embankment, indicating a potentially seepage problem.

At R1+700, a larger amount sand fill was placed to form the current embankment. Similarly, the embankment mainly composited of loose sand and lay on medium plastic clay. The thick foundation clay layer is judged to extend to the flood plain although the top layer of SPT-4 exhibits a sand layer. This sand layer could be moved from the embankment since this boring was drilled on the debris after the earthquake. The groundwater level obtained from the CPT indicates the high groundwater level in the embankment, possibly due to farmland behind the crest.

At R0+850 section, the failure here that only extended on the flood plain was different from the other two locations, where the entire embankment failed. Therefore, one boring and one CPT was drilled on the flood plain. The flood plain at R0+850 was gentle with a slope of less than 7.5° and mainly composited of soft clay. The foundation soil that extended to flood plain is also medium plastic clay, similar to the other two sections. While the embankment is mostly dry, the flood plain is submerged (saturated).

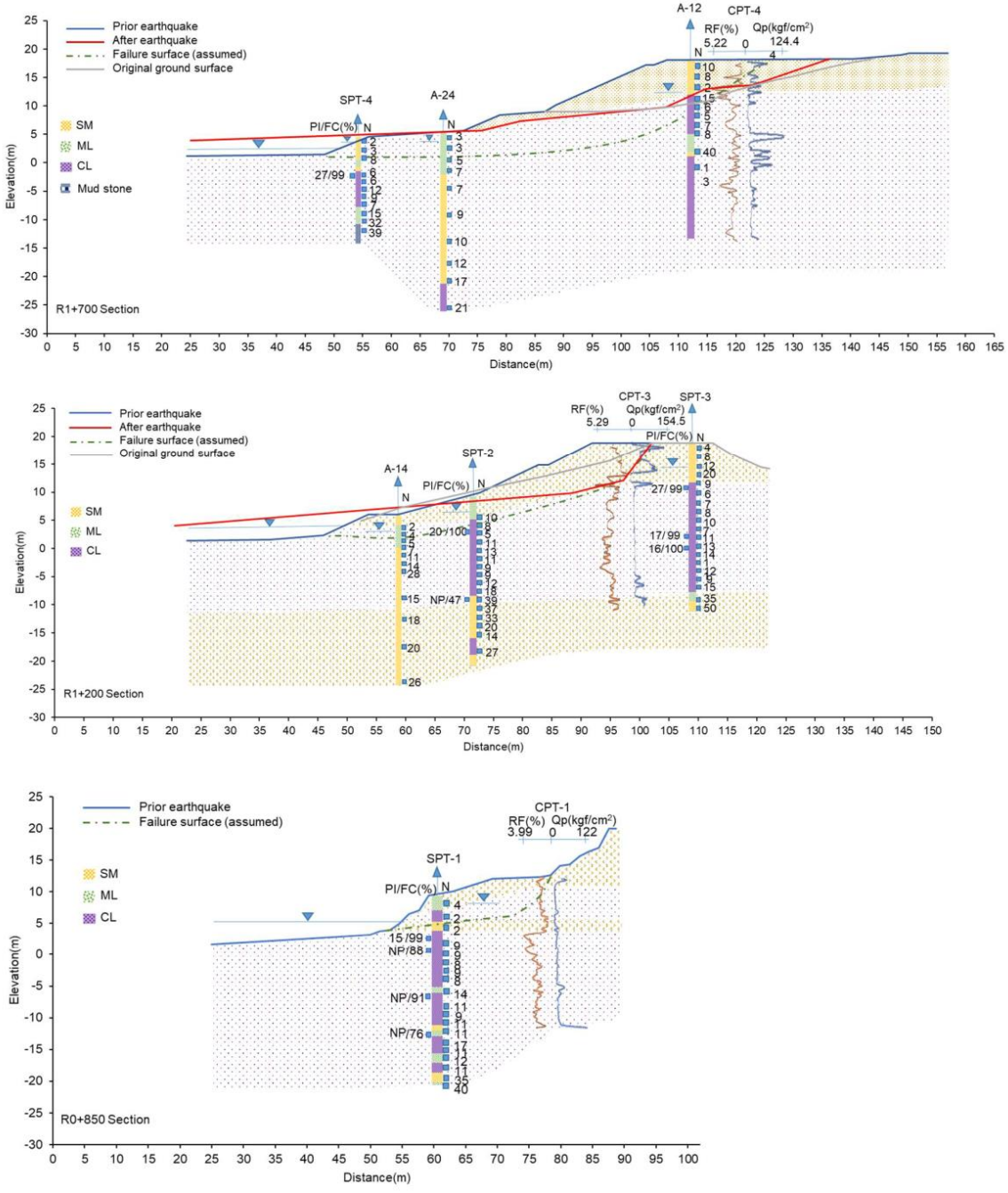

Figure 3. Subsurface characterization of R0+850, R1+200, and R1+700 section

3.2 *Failure plane and strength parameter*

The cross section prior to and after earthquake and the determined failure plane are shown Figure 3. At section R1+200 and R1+700 where significant failure occurred, the fill of the embankment was gone and piled up in the river. At section R0+850 where only tension cracks formed at the toe of embankment, the ground surface didn't have considerable change. Based on the ground surface prior to and after the earthquake, the failure surface of section R1+200 and R1+700 was assumed rationally. The sliding plane, determined based on the residual slope after the earthquake, staring from the crest of embankment, passing through the shallow part of the clay foundation, and extending to the toe of the flood plain. It was found that failure plane mostly went through the foundation clay layer. Therefore, this layer dominates the stability of this sections.

The strength properties of three main layers are listed in Table 2. The friction angle of sand layer is based on the SPT-N while the friction angle of clay layer is based the triaxial tests. The undrained shear strength of clay layer (Su/σv') determined as 0.40 is based the CPT and lab test results as shown in Figure 4.

Table 2. Strength of soil layers

Layer	c'	ϕ'	Su/σv'
Loose sand fill	0	32	-
Foundation clay	0	29	0.40
Foundation sand	0	36	-

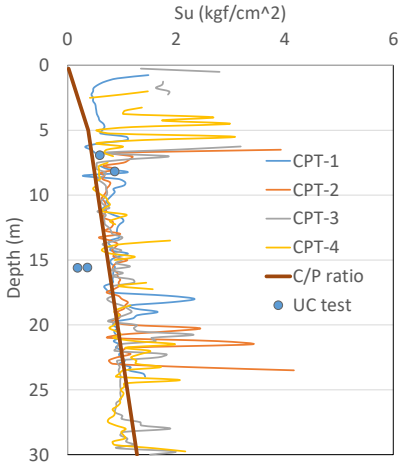

Figure 4. Undrained shear strength of clay layer

4 ANALYSIS METHODS

4.1 *Liquefaction analysis*

The semi-empirical SPT procedure by Hwang and Yang (2001) were adopted to evaluate the liquefaction potential. Besides, Boulanger and Idriss (2007) was used to evaluate the potential for cyclic softening (i.e., onset of significant strains or strength loss) in saturated silts and clays during earthquakes. The procedure is applicable for fine-grained soils with sufficient plasticity (PI>7) that they would be characterized as behaving more fundamentally like clays in undrained monotonic or cyclic loading.

Given that the energy ratio was not measured during the SPT test, the SPT-N was corrected to N_{60} (i.e. energy ratio of 60%) by assuming a measured energy ratio of 64% according to Huang (2008) based on analyses of 395 data of 24 borings conducted in Taiwan.

The liquefaction susceptibility criteria for silts and clays proposed by Boulanger and Idriss (2006) and Robertson (2009) were applied to distinguish between the sand- and clay-like soils for SPT and CPT data, respectively. For the SPT with PI measurement, the soil layers with PI > 7 (i.e., clay) were considered non-liquefied in the SPT-based approaches. For CPT sounding, soil behavior type index (Ic) values larger than 2.6 were considered non-liquefied. Those layers are analyzed following Boulanger and Idriss (2006) for the clayey like soil.

Su/sv' of 0.40 is used based on the CPT, laboratory test as shown in Figure 4. Therefore, OCR is approximated as 1.8 per (Ladd 1991).

The liquefaction analysis result is shown in Figure 5. FS of all borings is close to 1 near the top of clay layer (5-10 m). Note that the result is based on the assumption of K_α=1 (i.e. initial stress ratio is 0). However, for levees or slopes, initial stress ratio is not a unit and a correction factor less than 1 is required to reduce liquefaction resistance. Therefore, this result indicates those sections are marginally stable and was potentially onset of large strains. Moreover, those layers are corresponding the failure plane.

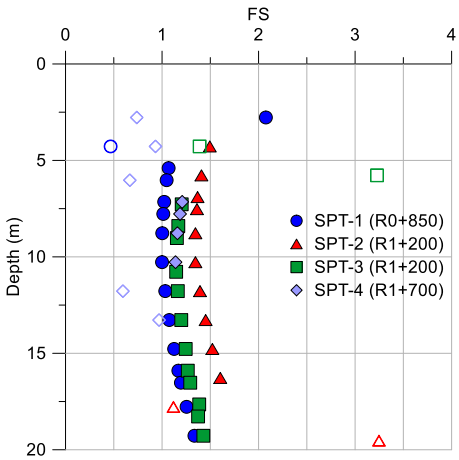

Figure 5. FS of liquefaction triggering analysis. Solid symbols indicate clayey soil and hollow symbols indicates sandy soil.

4.2 *Seepage and slope stability analysis*

Seepage and slope stability analysis are performed with the computer program SLOPE/W (GEO-SLOPE International Ltd.. 2012) for the static condition using the drained strength prior to the earthquake condition. The seepage analysis were first performed to obtain the phreatic line as shown in Figure 6 and then the slope stability analysis is performed to obtain the static FS of three sections. The result (Table 3) shows that FS is greater than 1, confirming the stability of these sections prior to the earthquake. However, the FS are close to one of R1+200 section, indicating marginally stable.

The yield accelerations (ky) of potential sliding blocks were then evaluated using limit-equilibrium analyses. Pseudo static analysis was performed with a predefined failure plane (according to Figure 3) along the top of the clay layer. Several iterations were required to find the yield acceleration of the failure plane at FS=1.0.

Strength softening of clay layer below the phreatic line, was considered using the simplified procedure proposed by (Tsai et al. 2014). The procedure has two main steps: (1) estimation of an equivalent cyclic shear strain amplitude and associated number of cycles induced in the soil mass by an earthquake; and (2) estimation of softening and strength loss in the soil mass. The detail information and the analysis result is shown in Table 4. It was found that the strengths of the saturated clay soils could be reduced by approximately 10-15 percent near the shallow clay layer given the shaking of 0.28g and Mw=6.4. The difference of

degrees of softening is mainly due to different stiffness (i.e. Vs obtained in the CPT soundings) and the depth. The yield accelerations (ky), obtained from pseudo static analyses using SLOPE/W for the no strength reduction and with different degrees of strength softening during the earthquake is summarized in Table 3.

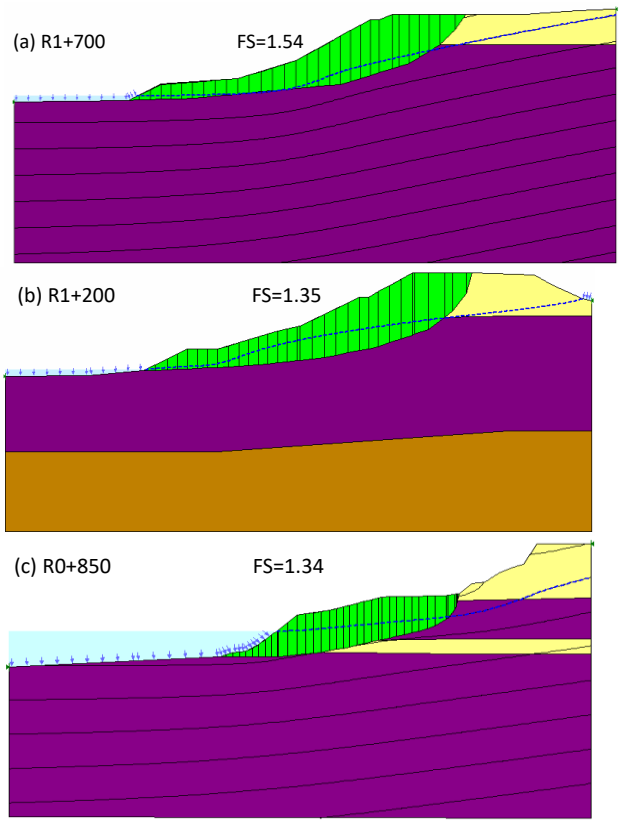

Figure 6. Seepage and static slope stability analysis result.

Table 3. Summary of FS and ky under different scenarios

Section	Pre-earth quake	During earthquake				
		No softening			With softening	
	FS	FS	ky	(%)	FS	ky
R1+200	1.71	1.35	0.10	10	1.20	0.06
R1+700	2.00	1.54	0.13	15	1.34	0.08
R0+850	1.44	1.34	0.09	15	1.19	0.05

Table 4. Information to estimate cyclic softening of clay soil

	Site/ soil condition			Estimated results			
	Vs	OCR	PI	N_c	γ_{eff}	$\gamma\gamma$	Softening
	m/sec	-	-	(-)	(%)	-	(%)
R1+200	180	1.8	16-27	11	0.08	0.90	10
R1+700	170	1.8	27	12	0.6	0.87	15
R0+850	150	1.8	15	13	0.6	0.85	15

4.3 *Newmark displacement analysis*

Seismically induced deformations of embankment were evaluated with Newmark-type procedures using the calculated yield accelerations and the recorded acceleration time history. Time history of is rotated to the transverse direction of the three failure section prior the analysis.

Displacements of the sliding block are calculated by integrating twice with time the difference between the earthquake-induced average acceleration of the slide mass and its yield acceleration with the computer program TNMN (Pyke 1992).The method is based on the assumption of rigid-perfectly plastic stress-strain behavior on a potential failure surface.

The time history of Newmark displacement is shown in Figure 7 and the total displacement is summarized in Table 5. It should be noted that the calculated Newmark displacement is an index and may not reflect the real displacement, especially not representing those (consequences) induced by the flow-type of failure. Typically, 5 cm is a threshold to trigger the failure of a slope. The estimated Newmark displacement is less than 5 cm expect for R1+200 without considering strength softening, indicating no failure occurred in these section. However, once the cyclic softening was considered, the estimated displacement is greater than 5 cm, consistent with the field observation of failure.

Table 5. Estimated Newmark displacement (m)

	No softening	With softening	Real
R1+200	0.03	0.17	55
R1+700	0.02	0.11	38
R0+850	0.06	0.17	30

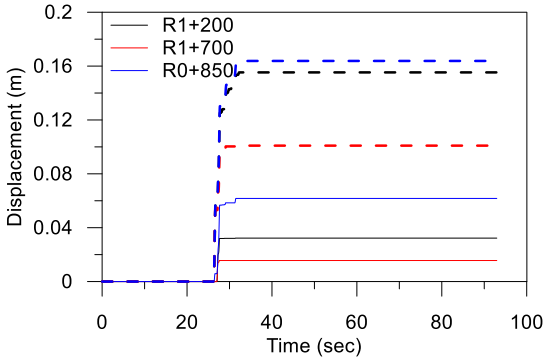

Figure 7. Time history of Newmark displacement with soften (das h line) and without softening (solid line).

5 CONCLUSION

This study investigates the three large scale failure of Rixin levee during the Meinong earthquake. The observed levee failure at three sections during reconnaissance right after earthquake was introduced. Additional field investigation and laboratory test were performed to characterize the embankment and foundation soil. Based on this information, liquefaction, seepage, slope stability analysis, and Newmark sliding block analysis were performed to gain insight of the failure mechanism.

Flow-type failure caused tremendous loss of levee and large amounts of debris almost blocked the flow channel of the river. The failure mechanism by soil liquefaction typically caused by sandy soil, however, fails to explain the case of Rixin levee because the foundation are primarily composed of clayey soil. By contrast, analysis result by Boulanger and Idriss (2006) indicates the potential for onset of significant strains or strength loss in saturated clays during earthquakes. Therefore, the cyclic softening of clayey soil subjected to cyclic loading is considered as a key factor to induce the damage. It wa found that when the strength of Rixin levee is reduced by about 10-15% accounting for cycle softening per Tsai et al. (2014), the estimated displacement of the embankment is in line with the observed damage of the levee.

6 ACKNOWLEDGEMENTS

This work was supported by the Ministry of Science and Technology in Taiwan, under Award No. 109-2625-M-005 -003

7 REFERENCES

Boulanger, R.W. & Idriss, I.M. 2006. Liquefaction susceptibility cr iteria for silts and clays. Journal of Geotechnical and Geoenvi ronmental Engineering, ASCE, **132**, 1413-1428.

Boulanger, R.W. & Idriss, I.M. 2007. Evaluation of Cyclic Softeni ng in Silts and Clays. Journal of Geotechnical and Geoenviro nmental Engineering, **133**.

Huang, F.-K. 2008. Establishment and application of the SPT eval uation model for the liquefaction probability and associated da mages. Journal of the Chinese Institute of Civil and Hydraulic Engineering, **20**, 155–174.

Hwang, J.H. & Yang, C.W. 2001. Verification of critical cyclic str ength curve by Taiwan Chi-Chi earthquake data. Soil Dynamic s and Earthquake Engineering 2001, 237-257.

Ladd, C.C. 1991. Stability evaluation during staged construction. J ournal of Geotechnical Engineering, **117**, 540-615.

GEO-SLOPE International Ltd. 2012.

Pyke, R. 1992. TNMN.

Robertson, P.K. 2009. Performance based earthquake design using the CPT. *IS-Tokyo 2009: international conference on perform ance-based design in earthquake geotechnical engineering—fro m case history to practice*, Tokyo, Japan, 15-18.

Tsai, C.-C., Hsu, S.-Y., Wang, K.-L., Yang, H.-C., Chang , W.-K., Chen, C.-H. & Hwang, Y.-W. 2017. Geotechnical Reconnaissa nce of the 2016 ML6.6 Meinong Earthquake in Taiwan. Journ al of Earthquake Engineering.

Tsai, C.-C., Mejia, L.H. & Philip, M. 2014. A strain-based proced ure to estimate strength softening in saturated clays during ear thquakes. Soil Dynamics and Earthquake Engineering, **66**, 191-198.